



## Performance comparison of differently dried graphene oxide-based membranes for desalination by forward osmosis

Abdulahkim Alhinai<sup>a,b</sup>, Mohamed Edokali<sup>a</sup>, Louey Tliba<sup>a</sup>, Robert Menzel<sup>c</sup>,  
Ali Hassanpour<sup>a,\*</sup>

<sup>a</sup> School of Chemical and Process Engineering, Faculty of Engineering and Physical Science, University of Leeds, Leeds LS2 9JT, UK

<sup>b</sup> Department of Chemical and Petrochemical Engineering, University of Nizwa, P.O. Box 33, Oman

<sup>c</sup> School of Chemistry, Faculty of Engineering and Physical Science, University of Leeds, Leeds LS2 9JT, UK

### ARTICLE INFO

#### Keywords:

Graphene oxide membrane  
Forward osmosis  
Water desalination  
Freeze-drying  
Oven drying  
Vacuum drying

### ABSTRACT

This study aims to explore the influence of freeze-drying (FD), vacuum-drying (VD), and oven-drying (OD) on the physicochemical properties, structural integrity, and desalination efficiency of graphene oxide (GO) membranes in Forward Osmosis (FO). Mixed cellulose ester (MCE) membranes were modified with thin GO active layers, optimised by the design of experiments (DoE) protocol, without the use of additional chemical coupling or crosslinking additives. Membranes were fabricated using commercial GO dispersions, followed by drying under the three methods, and then characterised to determine their physicochemical and morphological properties. The results demonstrated that the drying method had a significant impact on the properties of GO membranes: FD effectively preserved the structural framework and functional groups; VD led to moderate deoxygenation; and OD resulted in pronounced structural compaction and extensive loss of oxygen-containing functionalities. Consequently, FD-GO exhibited high hydrophilicity, VD-GO showed moderate hydrophilicity, and OD-GO displayed reduced wettability. The findings also revealed that FD-GO membranes exhibited high water flux, achieving up to 11.28 L/m<sup>2</sup>.h at a low GO concentration (0.033 mg/mL), due to their preserved porous structure and high hydrophilicity. In contrast, OD-GO membranes showed the highest salt rejection rates, up to 99.67 % at 1 mg/mL concentration, attributed to their compact structure and smaller interlayer spacing due to the loss of oxygen groups. VD-GO membranes provided a balance between water flux and salt rejection, demonstrating intermediate performance. These results suggest that optimal drying techniques can significantly impact the design and scalability of next-generation GO-based FO membranes, enabling efficient, environmentally friendly, chemical-free desalination solutions suitable for industrial applications.

### 1. Introduction

Membrane separation technology has gained significant attention for water purification and desalination due to its advantages of low energy consumption, cost-effectiveness, straightforward fabrication, and continuous operational capabilities (Tian et al., 2020; Huang et al., 2021; Meng et al., 2020). Despite these benefits, critical parameters such as permeability and selectivity continue to hinder its advancement (Marchetti et al., 2014; Warsinger et al., 2018). Recent efforts in

membrane research have prioritised the development of materials that enhance both selectivity and permeability (Zhang et al., 2021). Exploring innovative membrane processes and novel materials is regarded as a pivotal approach for advancing alternative water treatment solutions (Ibraheem et al., 2023; Nde et al., 2023). Forward osmosis (FO), as an emerging membrane technology, has demonstrated considerable promise for seawater desalination compared to other pressure-driven methods, attributed to its potential for reduced energy consumption (Goh et al., 2016; Edokali et al., 2023). Nevertheless,

**Abbreviations:** C<sub>12</sub>H<sub>22</sub>O<sub>11</sub>, Sucrose; GO, Graphene Oxide; FO, Forward Osmosis; FD, Freeze-Drying; VD, Vacuum-Drying; OD, Oven-Drying; Å, Angstrom scale; FTIR, Fourier Transform Infrared; XRD, X-ray Diffraction; SEM, Scanning Electron Microscopy; WCA, Water Contact Angle; ZP, Zeta Potential; MCE, Mixed Cellulose Ester; DIW, Deionised Water; FS, Feed Solution; DS, Draw Solution; DOE, Design of Experiments; LMH, Liters per Square Meter per Hour; NaCl, Sodium chloride; pDA, Polydopamine; PVDF, Poly(vinylidene difluoride); R<sub>s</sub>, Salt rejection efficiency; RT, Room temperature.

\* Corresponding author.

E-mail address: [A.Hassanpour@leeds.ac.uk](mailto:A.Hassanpour@leeds.ac.uk) (A. Hassanpour).

<https://doi.org/10.1016/j.ces.2025.121998>

Received 7 December 2024; Received in revised form 15 May 2025; Accepted 6 June 2025

Available online 7 June 2025

0009-2509/© 2025 The Authors. Published by Elsevier Ltd. This is an open access article under the CC BY license (<http://creativecommons.org/licenses/by/4.0/>).

practical implementation of FO desalination is impeded by persistent challenges, including low water flux, reverse solute flux, membrane fouling, and significant internal concentration polarisation (ICP) (Zhao et al., 2012). These issues are predominantly associated with the limited use of commercial polymeric membranes, which restricts the overall desalination performance (Ndiaye and Vaudreuil, 2019). Consequently, there is an urgent need for the development of novel membrane materials that can enhance FO performance in desalination applications.

In recent years, two-dimensional (2D) materials, such as graphene and related nanosheets, have shown significant potential for high-performance separation membranes due to their layered structures that are conducive to modification and molecular separation (Nde et al., 2023; Yang et al., 2022; Xiao et al., 2021). Graphene, in particular, stands out for its remarkable mechanical strength, chemical stability, exceptional electrical and thermal conductivity, and high specific surface area (Allahbakhsh and Arjmand, 2019; Surwade et al., 2015). Among its various derivatives, graphene oxide (GO) has emerged as especially significant. With its single-atom-layer thickness and an abundance of oxygen-containing functional groups, including hydroxyl, carboxyl, and epoxy groups, GO lends itself well to chemical modification and large-scale applications (Dreyer et al., 2010; Gao et al., 2009). Current research has focused on enhancing the performance of GO-based membranes for FO desalination, aiming to balance the trade-off between flux and rejection while reducing production costs to enable large-scale industrial use (Wang et al., 2023; Edokali et al., 2024; Edokali et al., 2024). Key improvements in separation efficiency have been achieved by optimising the degree of oxidation (i.e., reduction or loss of oxygen functional groups) and fine-tuning functional groups to regulate interlayer spacing, thereby elucidating the mechanisms of molecular separation (Nde et al., 2023; Edokali et al., 2023; Jabbari et al., 2023). Studies have demonstrated the high selectivity and permeability of GO-based membranes, solidifying their candidacy for FO water purification (Wu et al., 2020; Castelletto and Boretti, 2021).

GO-based FO composite membranes can be synthesised through various techniques, including vacuum/pressure-driven filtration (Song et al., 2019; Deka et al., 2021), drop-casting (Balapanuru et al., 2019), spin-coating (Kim et al., 2017; Talar et al., 2019), layer-by-layer assembly (Salehi et al., 2017), and electrophoretic deposition (Edokali et al., 2024; Fan et al., 2019), each with unique properties. Precise control of the transport channels at the angstrom scale (Å) is essential for effective molecular separation. The interlayer spacing in GO membranes has been identified as a crucial factor influencing molecular transport and can be adjusted through chemical and physical modifications (Su et al., 2020). Chemical tuning involves the incorporation of functional molecules or cations to crosslink GO layers and fix interlayer spacing (Chen et al., 2017). However, the use of chemical additives introduces potential risks and can compromise the membrane's structural integrity, limiting backwash sustainability in FO processes (Wu et al., 2020).

On the other hand, physical methods such as external pressure applications and physical fixation have shown promise in preventing out-of-plane swelling and accurately tuning interlayer spacing. These methods enhance stability, enable rapid water transport, and improve salt rejection (Su et al., 2020; Li et al., 2018). For example, Joshi et al. fabricated laminar GO-based membranes using vacuum filtration and studied the selective transport of ions and molecules through concentration-driven diffusion (Joshi et al., 2014). Their GO membranes, with a thickness of 5 mm, exhibited precise molecular sieving with a cutoff at approximately 9 Å. Physical confinement techniques have also been effective in controlling out-of-plane swelling and optimising interlayer spacing. As such, Abraham et al. employed epoxy to encapsulate stacked GO laminates, creating mechanically stabilised membranes resistant to expansion in water or humid environments (Abraham et al., 2017). These membranes, with a d-spacing of 6.4 Å, demonstrated high salt rejection, successfully preventing Na<sup>+</sup> and K<sup>+</sup> ions from passing through even after prolonged exposure.

While the properties and potential applications of GO-based

nanomaterials have been extensively studied, a significant gap remains in the literature regarding the comparative analysis of different drying methods used in the fabrication of GO-based membranes. In this context, research predominantly focuses on the chemical and physical properties of these membranes, such as their enhanced permeability and mechanical strength, often neglecting the impact that drying processes may have on these characteristics (Nde et al., 2023; Wang et al., 2023; Wu et al., 2020; Castelletto and Boretti, 2021). Future research should expand upon physical confinement strategies by exploring a range of drying methods to enhance the stability and transport characteristics of GO-based FO membranes. This includes vacuum drying, oven drying, and freeze drying, distinctly influencing the structural integrity, functional efficacy, and overall performance of FO membranes, which have yet to be fully investigated. The drying technique is crucial as it can affect the distribution of functional groups, interlayer spacing, and ultimately, the membrane's performance in terms of water flux and salt rejection.

In this study, a strategy has been followed to create additive-free, fairly-stable, and charged GO-based FO membranes without any chemical modification. This approach involved a comparative analysis of vacuum-dried (VD), oven-dried (OD), and freeze-dried (FD) GO films for FO desalination applications. The initial concentration and loading of GO for membrane fabrication were optimised using a design of experiments (DoE) protocol. To the best of our knowledge, this represents the first systematic study of these three drying methods in context of additive-free GO-FO membrane fabrication. While long-term membrane operation is essential for practical applications, the present study focuses on the short-term FO performance of pristine GO-based membranes to isolate and evaluate the effects of different drying methods on their intrinsic physicochemical stability and transport characteristics without interference from additives or chemical crosslinkers which could critically influence early-stage water flux and salt rejection. Comprehensive analysis of GO deposition, concentration, and fabrication methodologies was conducted, followed by detailed physicochemical and morphological characterisations to assess surface properties and performance. The desalination capabilities of the GO-based membranes were evaluated using a laboratory-scale FO setup. The findings from this research could contribute to the design and scalable production of next-generation GO-FO membranes.

## 2. Experimental

### 2.1. Materials and methods

Graphene oxide, in a colloidal suspension with a concentration of 1.03 % and a pH of less than 2, was supplied from William Blythe Ltd – UK. Sodium chloride (NaCl, molecular weight 58.44 g/mol) and sucrose (C<sub>12</sub>H<sub>22</sub>O<sub>11</sub>, molecular weight 342.3 g/mol) were purchased from Sigma-Aldrich – UK. Support filtration membranes of mixed cellulose ester (MCE, 47 mm diameter, 65 – 85 % porosity, and approximately 70 μm thickness) purchased from Scientific Laboratory Supplies (SLS – UK). All aqueous solutions were prepared using deionised water (DIW) from a Millipore system, showcasing a resistivity of 18.3 MΩ/cm at 25 °C. All chemicals used in this study were of reagent grade and were used without further purification.

### 2.2. Fabrication procedure of GO-based membranes

Aqueous GO dispersions were prepared at three different concentrations (0.033 mg/ml, 0.1 mg/ml, and 1 mg/ml), with each concentration used at two different volumes (2 ml and 4 ml), to enable optimisation of membrane fabrication via a systematic DoE approach. In this work, the GO concentrations and drying conditions of all membranes were selected based on a systematic optimisation study (as thoroughly explained in Section S1, SI). These parameters were found to fabricate membranes with the most favourable mechanical

robustness, and desalination performance.

To ensure a homogeneous mixture and prevent any contaminations or aggregations, controlled amounts of GO were dispersed in DIW at 800 RPM for 2 mins using a magnetic stirrer (Asynt, ADS-HP-NT hotplate stirrer), followed by 10 mins of sonication in a water bath (BRANSONIC 2800-E CPX ultrasonic water bath) at room temperature ( $\approx 25^\circ\text{C}$ ). The resultant dispersions were then used for the fabrication of the GO membranes. The fabrication process of GO-based membranes commenced with the initial preparation of the membrane film, which involved wetting the MCE support film in DIW to ensure adequate hydration and flexibility for handling. Once sufficiently wet, the support membrane was carefully transferred to a vacuum filtration setup, where additional DIW was poured to facilitate the uniform coverage of the GO dispersion across the substrate. The dispersion of GO was then slowly introduced onto the wet support membrane under vacuum conditions at 0.1 bar to ensure an even deposition of GO onto the membrane surface. Following the drying process, three distinct methods were employed to further process the membranes: oven-drying (OD), vacuum-drying (VD),

and freeze-drying (FD). The freeze-drying process involved freezing the membrane (*denoted as GO-FD*) at a controlled temperature of  $-50^\circ\text{C}$  for 4 hrs. using a LABCONCO FreeZone Benchtop Freeze Dryer. Subsequently, the membrane was subjected to vacuum conditions to sublimate the formed ice, thereby preventing collapse of the porous structure and preserving the integrity of the deposited GO layer. In contrast, the vacuum-drying process involved drying the membrane (*denoted as GO-VD*) in a GALLENKAMP Fistream vacuum oven at a controlled temperature of  $120^\circ\text{C}$  for 3 hrs. This optimised procedure facilitated the gradual removal of residual moisture and contributed to the formation of more stable GO structures (refer to **Section S1, SI**). On the other hand, the oven-drying process involved placing the membrane (*denoted as GO-OD*) in a conventional oven (Binder ED23,  $300^\circ\text{C}$  laboratory oven) under an air atmosphere at a controlled temperature of  $120^\circ\text{C}$  for 2 hrs. Each drying method was optimised (see **Section S1, SI**) to enhance the mechanical properties and filtration efficiency of the resulting GO membranes, thereby making them suitable for advanced water purification in FO applications. For analytical comparison, a pristine GO

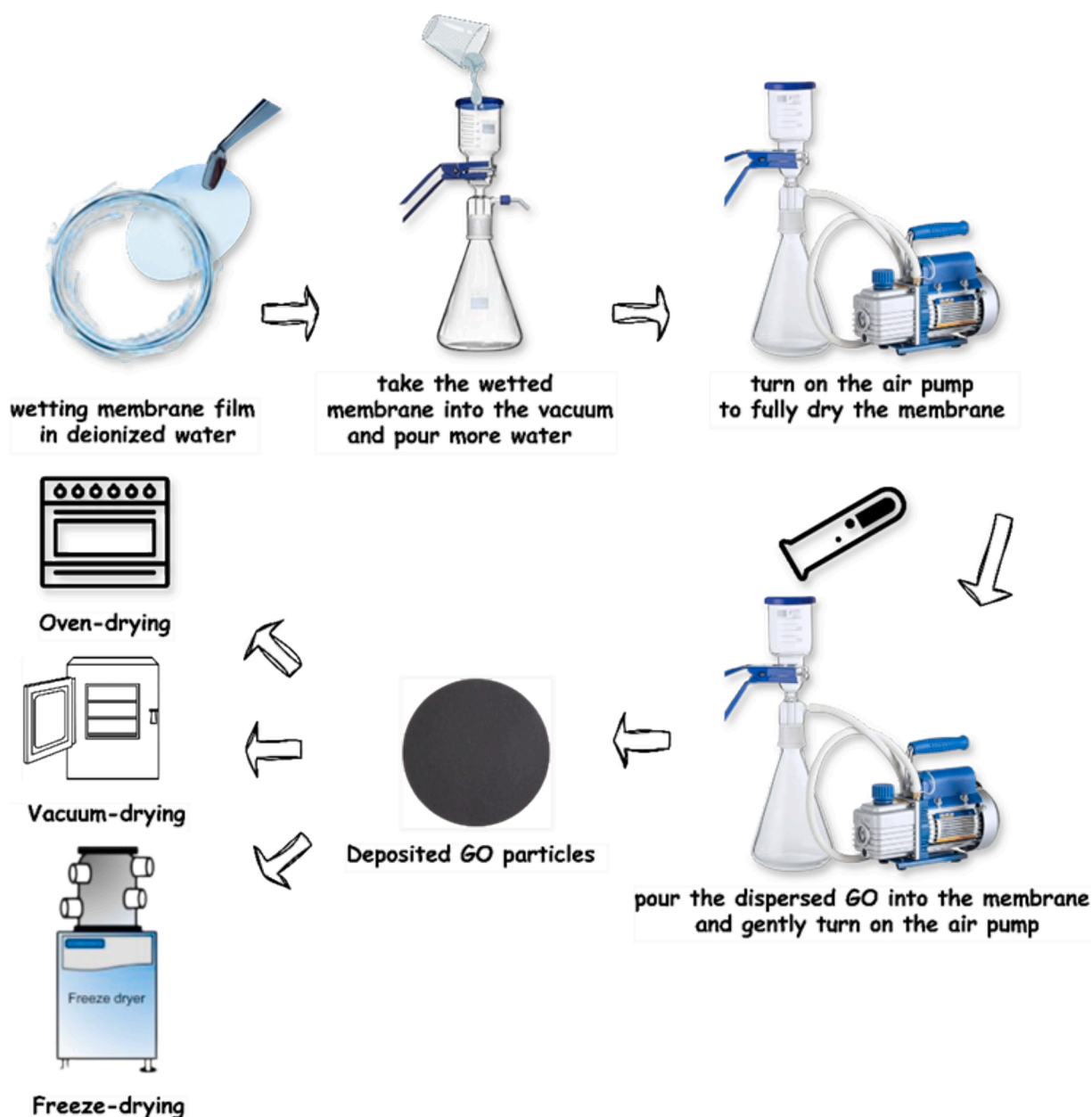


Fig. 1. Schematic diagram of fabrication and drying processes of GO-based membranes.

membrane (denoted as *Pristine GO*) was also prepared by vacuum-filtering a GO dispersion onto an MCE substrate at 0.1 bar, followed by complete drying at room temperature. Finally, all resulting membranes were stored in a desiccator under an inert gas for further use. The schematic for formulation process of membranes is shown in Fig. 1.

## 2.3. Physicochemical and morphological characterisation

### 2.3.1. X-ray diffractometer (XRD)

X-ray Diffraction (XRD) analysis of membranes was conducted using a Bruker D2 X-ray diffractometer equipped with a Cu-K ( $\alpha$ ) radiation source (wavelength,  $\lambda = 1.5418 \text{ \AA}$ ). The X-ray diffractometer was operated at a constant voltage of 30 kV and current of 10 mA. Each XRD scan lasted for 20 mins, during which the sample was rotated at a speed of 30° per min. The XRD measurements covered a  $2\theta$  angle range from 5 to 80°, with a step size resolution of 0.02°, and each step took approximately 41.3 s. To minimise the background interference from the MCE support, the XRD profiles of GO-supported membranes were slightly baseline-corrected and normalised. For clarity, all patterns were grouped in a single plot to enable direct comparison of GO peak shifts and structural variations induced by different drying methods.

### 2.3.2. Fourier transform infrared (FTIR) spectroscopy

Membrane samples were subjected to Fourier Transform Infrared (FT-IR) spectroscopy using a Bruker Platinum equipped with a diamond Attenuated Total Reflectance (ATR) accessory. The measurements were performed in transmission mode, covering a wavelength range of 400 to 4000  $\text{cm}^{-1}$ . Each sample underwent 16 scans, and the spectral resolution was set at 4  $\text{cm}^{-1}$ .

### 2.3.3. Surface morphology (SEM)

Scanning electron microscopy (SEM) using an TM3030Plus instrument was employed to comprehensively analyse the surface characteristics of the membrane specimens. In advance of SEM imaging, all samples were particularly mounted onto specialised aluminium SEM stubs, followed by a carbon coating process utilising an ion sputtering device for a duration of 3 mins. SEM images were acquired utilising the normal lens mode, with operational parameters set at an accelerating voltage of 5.0 kV (with emission current 16,800nA and filament current 1750 mA), and an optimal working distance of 6.9 mm.

### 2.3.4. Water contact angle (WCA)

Contact angle measurements of membranes were conducted to quantitatively assess the wettability of the surfaces of the variously prepared GO membranes on a dynamic basis. The measurements were performed using a Biolin Scientific Attension Theta Flex optical tensiometer, employing the sessile droplet method. To analyse the effect of drying on the wettability of the membranes, the contact angles between the membrane surface, water droplet, and air were measured. The contact angle was recorded at specific time intervals over a duration of 80 s, focusing on the interaction with the high-density phase (water). A 5.5  $\mu\text{L}$  droplet of DIW was carefully placed on the membrane surface for each measurement. To ensure the reliability of the data, each measurement was repeated three times at different locations on the membrane, providing a robust assessment of droplet stability and results.

### 2.3.5. Zeta potential (ZP)

Zeta potential measurements as a function of pressure drop were conducted using a SurPASS 3 instrument (Anton Paar). Membrane samples were cut into strips measuring 1.5 cm  $\times$  3 cm and mounted onto the sample holder within the adjustable gap cell for disks (10  $\times$  20 mm) using double-sided adhesive tape. The electrolyte solution used was 0.1 M NaCl, with a pH of 5.55, conductivity of 1.07 S/m, and a temperature maintained at 26.44°C. The sample holder with the mounted membranes was installed into the measuring cell, adjusting the gap height of 94  $\mu\text{m}$  to create a stable flow channel. The cell was filled with

the electrolyte solution, ensuring consistency with the provided conditions for FO desalination experiments. Data was collected through the SurPASS 3 software, capturing the zeta potential as a function of the applied average pressure drop.

## 2.4. Evaluation of membrane performance in forward osmosis testing setup

The experimental configuration for the FO setup (refer to Fig. 2) was carefully devised to assess the efficiency of the three differently dried GO membranes in the process of water purification. The laboratory-scale system employs precision weighing scales (AND EK-3000i Compact, A&D Weighing) capable of accurately measuring and recording mass changes in both the feed and draw solution beakers, with a precision of

$\pm 0.1 \text{ g}$ . This level of precision guarantees a precise measurement of water flux through the membrane. During this study, the active layer of the resultant GO membranes was positioned towards the feed solution (FS) while the support layer faced the draw solution (DS), replicating the usual FO operation in desalination mode. The feed and draw solutions were circulated through a CF-042P-FO membrane cell, with 6.16  $\text{cm}^2$  membrane effective area, using peristaltic pumps (Model: 07555-15, Masterflex™, Cole-Parmer) at a flow rate of around 220 mL/min. For each membrane test, the FO system was continuously operated for 1 hr. following stabilisation of the flow. In addition, the temperatures of the feed and draw solutions were precisely regulated using temperature sensors, ensuring that all tests were conducted under stable thermal conditions conducive to reliable data collection. The water flux ( $J_w$ , LMH) of membranes was calculated using the following equation (Jang et al., 2020):

$$J_w = \frac{\Delta V}{A \times \Delta t} \quad (1)$$

Where ( $\Delta V$ ) is the volume change of the feed solution using a constant density of DIW ( $\rho$ ) permeated across the effective area of the membrane ( $A$ ) and measured over a time interval ( $\Delta t$ ) at which the measurement was taken every 5 mins for each single membrane..

For salt rejection testing, 0.5 L of a 0.5 M sucrose solution was used as the draw solution. Its conductivity was measured using a conductivity meter (FiveEasy™ Plus FP30, Mettler Toledo) with a precision of 0.1 ppm. Simultaneously, the concentration of the feed solution, consisting of 0.5 L of a 0.1 M NaCl solution, was measured at both the beginning and the end of the FO salt rejection tests. This enabled the calculation of the salt rejection percentage ( $R_s$ , %), providing a comprehensive assessment of the membrane's effectiveness for desalination. This can be calculated using the following equation (Jang et al., 2020):

$$R_s = \left(1 - \frac{C_p}{C_f}\right) \times 100 \quad (2)$$

Where ( $C_p$ ) is the salt concentration in the permeate side and ( $C_f$ ) is the salt concentration in the feed solution, both determined through conductivity measurements.

## 3. Results and discussion

### 3.1. Characterisation of additive-free modified GO-based membranes

Various characterisation techniques were employed to investigate the physicochemical and morphological changes in GO resulting from the different drying methods as described in the methodology section. The XRD was used to examine structural alterations in both the commercial MCE substrate and the GO-based membrane samples under varying drying conditions (Fig. 3 (a)-(c)). For comparison, the distinctive and typical XRD profile of the cellulose MCE membrane is shown in Fig. 3 (a). The XRD pattern of the commercial MCE membrane showed a

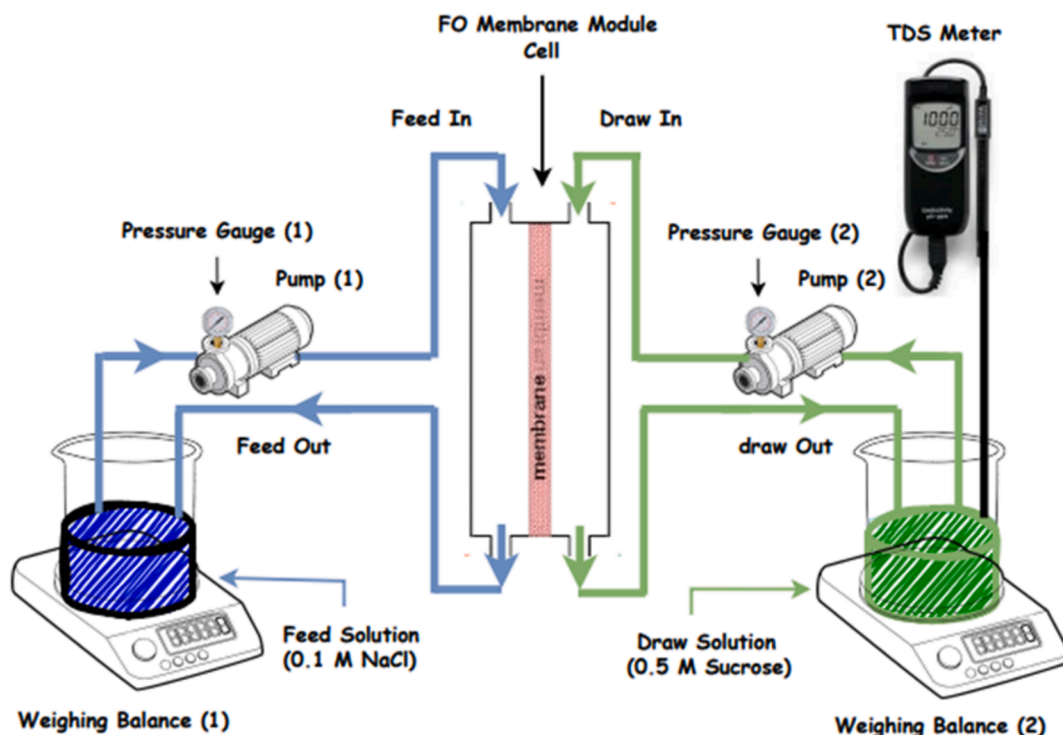


Fig. 2. Schematic of the forward osmosis experimental setup.

pattern with multiple peaks, suggesting a crystalline structure. (Mohiuddin et al., 2015; Kamal et al., 2018; Li et al., 2024). In the pristine GO sample, as displayed in Fig. 3 (b), the peak at  $2\theta = 9.64^\circ$  presented an interlayer spacing of 0.92 nm (refer to Table S2, SI). The presence of oxygen-containing functional groups and intercalated water molecules in GO contributes to the observed expansion in interlayer spacing, as evidenced by the characteristic XRD peak. This increased spacing facilitates the incorporation of polar functional groups and water molecules, enabling GO to disperse readily in aqueous solutions (Nde et al., 2023; Chong et al., 2016; Zhu et al., 2022).

After drying, all fabricated GO samples (i.e., FD, VD, and OD) exhibited a shift in the (002) GO peak toward higher  $2\theta$  values, indicating deoxygenation of the GO and a corresponding reduction in interlayer spacing, as shown in Fig. 3 (c). This peak shift indicates the effective removal of oxygen-containing functional groups, allowing the graphene sheets to align more compactly. The extent of the shift varied among the samples, reflecting different degrees of deoxygenation depending on the drying method employed (Nde et al., 2023; Jabbari et al., 2023; Pei et al., 2016). In terms of drying methods comparison, the FD samples, as shown in Fig. 3 (c), displayed shifts in  $2\theta$  values ranging from 11.25 to 11.56, with corresponding interlayer spacings between 0.77 and 0.79 nm (refer to Table S2, SI). These findings suggest that freeze-drying was more effective in preserving the GO structure, likely due to its low-temperature, sublimation-based drying mechanism, which helps prevent structural collapse (Ham et al., 2014). In contrast, the VD samples, as shown in Fig. 3 (c), exhibited  $2\theta$  values ranging from 11.96 to 12.47, corresponding to interlayer spacings of 0.71 to 0.74 nm. These results indicate that vacuum drying led to greater deoxygenation and loss of interlayer water in GO compared to freeze-drying, but to a lesser extent than oven drying. Further, the oven-OD samples, as shown in Fig. 3 (c), exhibited a shift in  $2\theta$  values ranging from 12.47 to 13.68, corresponding to a decrease in interlayer spacing to between 0.66 and 0.71 nm. Notably, this pronounced decrease suggests that oven drying was more effective in removing oxygen-containing functional groups, despite the fact that the same drying temperature of 120 °C was used for both vacuum-oven and conventional-oven drying (Edokali

et al., 2023; Edokali et al., 2024; Deka et al., 2021). The distinct structural characteristics of the GO membranes demonstrate that interlayer spacing can be effectively tuned through the choice of drying method alone, an important consideration for the application of GO-based FO membranes in water purification and filtration.

Fig. 4 (a) shows the FTIR spectrum of the pristine MCE support membrane with distinctive chemical functional groups, consistent with those reported in the literature (Ghahari et al., 2024). The FTIR spectrum of the pristine GO membrane, as depicted in Fig. 4 (b), exhibited several characteristic peaks corresponding to various oxygen-containing functional groups. In this sample, the presence of hydroxyl groups and intercalated water molecules was indicated by the broad peak about  $3400\text{ cm}^{-1}$ , due to O-H stretching vibrations, which agreed with reported literatures (Edokali et al., 2023; Deka et al., 2021). A prominent peak at approximately  $1720\text{ cm}^{-1}$  corresponded to C=O stretching vibrations, indicating the presence of carboxyl groups. Other peaks in the range of  $1000\text{--}1300\text{ cm}^{-1}$  were associated with C-O stretching vibrations of epoxy and alkoxy groups. Additionally, the peak observed around  $1620\text{ cm}^{-1}$  was attributed to the skeletal vibrations of unoxidised graphitic domains (C=C) (Parsamehr et al., 2019).

More pronounced changes in the FTIR spectra generally corroborated the XRD findings, confirming varying degrees of GO deoxygenation resulting from the three different drying methods. For the FD samples (FD-0.033, FD-0.1, FD-1), as shown in Fig. 4 (c), the FTIR spectra revealed moderate de-oxygenation and hence reduction in the intensity of the O-H stretching peak compared to pristine GO, as indicated by XRD patterns in Fig. 3. The O-H stretching peak around  $3400\text{ cm}^{-1}$  decreased in intensity but remained present, indicating loss of interlayer water and suggesting a partial degree of GO deoxygenation (Yang et al., 2017). As expected, freeze-drying preserved more of the original GO structure, including some hydroxyl groups. On the other hand, the VD samples (VD-0.033, VD-0.1, VD-1), as depicted in Fig. 4 (c), showed an intermediate level of reduction in the intensity of the O-H stretching peak around  $3400\text{ cm}^{-1}$ , compared to that of freeze-drying and oven-drying. This suggests that vacuum-drying could provide a balance between preserving the original structure and achieving

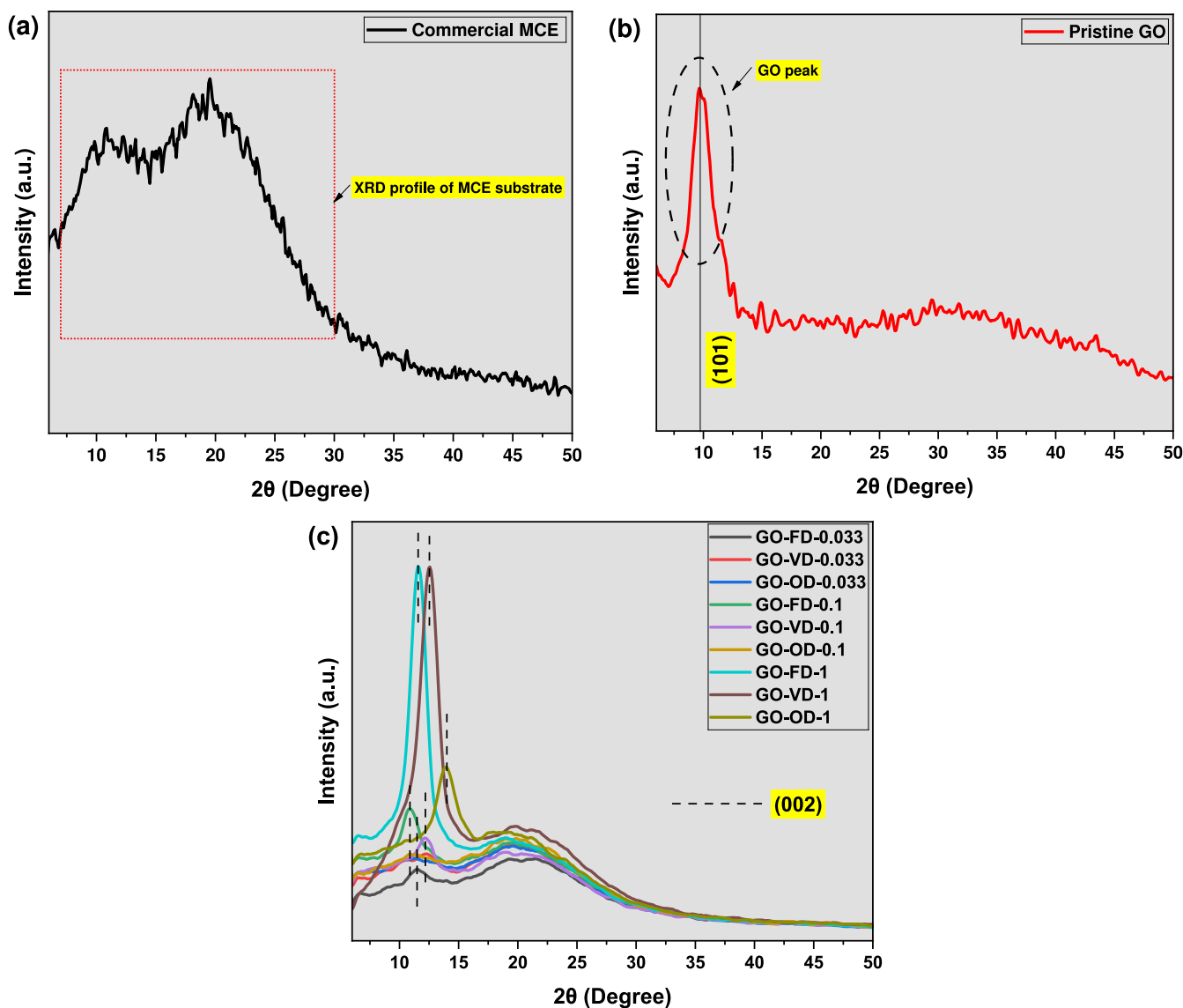


Fig. 3. XRD profiles of (a) commercial MCE, (b) pristine GO-based membranes, and (c) d-spacing shifts of the three drying methods on the GO.

effective reduction degree of the GO de-oxygenation (Wu et al., 2020; Yang et al., 2017). Hereby, this approach removed some interlayer water, leading to a partially reduced graphene structure. In comparison, the OD samples (OD-0.033, OD-0.1, OD-1), as shown in Fig. 4 (c), exhibited the most significant reduction in the intensity of the O-H stretching peak. This proposed more loss of oxygen functional groups and intercalated water (Liu et al., 2015). This substantial decrease could result in a more reduced form of graphene.

Scanning electron microscopy (SEM) was used to characterise the surface topography and morphology of the pristine GO membrane and GO-based membranes prepared using different drying methods, as shown in Fig. 5. As can be observed in Fig. 5 (a-I) and (a-II), the commercial MCE substrate demonstrated a highly porous and rough surface (Ghahari et al., 2024; Zhu et al., 2021). After deposition of GO-based laminates, the microstructures of pristine GO- and variously dried GO-supported membranes varied significantly, as revealed by SEM observations, with each drying method significantly impacting the texture and final characteristics of GO materials. Generally, all GO-based membranes exhibited a typically wrinkled-like structure (Yuan et al., 2017). In their pristine state, as seen in Fig. 5 (b-I) and (b-II), the GO membranes exhibit a more wrinkled structure, attributed to the extensive oxidative treatments applied during synthesis (Wu et al., 2020). GO

membranes treated with freeze-drying, Fig. 5 (c), (f) and (i), showed generally fully intact GO layers with a relatively high density of the wrinkles. Vacuum-dried GO samples, as shown in Fig. 5 (d), (g) and (j), exhibited a denser wrinkle structure, consistent with more pronounced deoxygenation and partial restructuring of the original GO layers, which may have led to compression of the deposited GO layers during vacuum oven drying. On the other hand, the conventionally oven-dried samples, shown in Fig. 5 (e), (h), and (k), exhibited significant morphological changes, with tightly packed and flattened layers clearly visible. These features were consistent with more pronounced deoxygenation, leading to a degree of re-lamination of the GO layers. These findings can be significant to tailor the characteristics of differently dried GO membranes for separation applications, with additional potential for reducing membrane fouling through control of GO membrane surface texture.

The surface wettability also plays an important role in the desalination efficiency of GO-based membranes (Edokali et al., 2024). Water contact angle (WCA) is an essential measurement in determining the interactions of liquid with a solid surface, providing an insight of the wettability degree and surface energy. The dynamic contact angle measurements, presented in Fig. 6, offer a comprehensive analysis of the wettability of GO-based membranes subjected to different drying

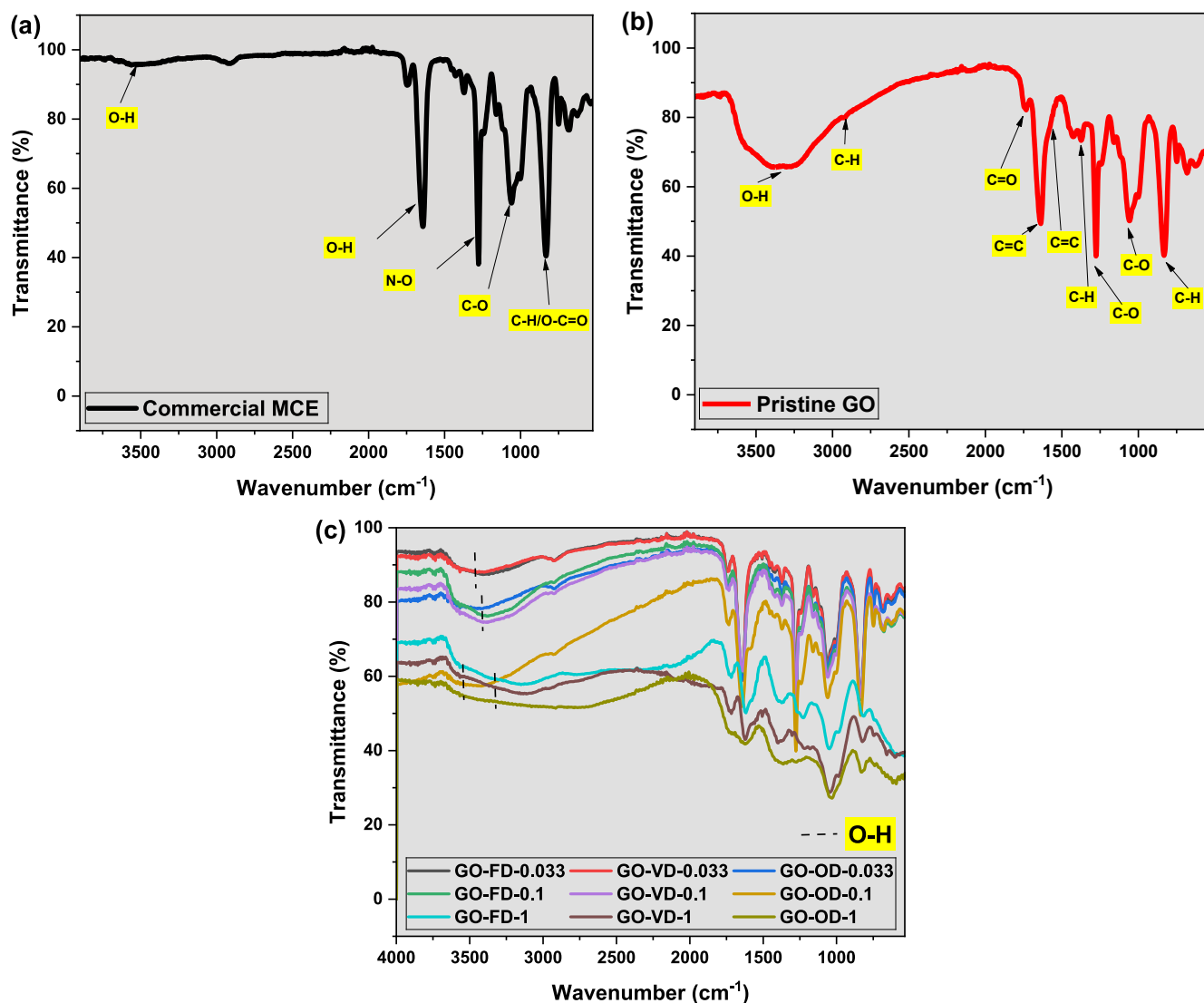


Fig. 4. FTIR Spectra of (a) commercial MCE, (b) pristine GO-based membranes, and (c) schematic of the effect of the three drying methods on the GO-based films.

methods, in comparison to pristine GO and porous MCE membranes. The findings revealed significant differences in the hydrophilicity of these membranes, which can be attributed to the specific drying methods used. The first contact angle measurements, shown in Fig. 6 (a), compared the pristine GO membrane with a commercial MCE support membrane. Clearly, the pristine GO membrane exhibited a relatively high initial contact angle that gradually decreased over time, indicating moderate wettability. The commercial MCE substrate, showed a significant reduction in contact angle, suggesting higher initial hydrophilicity due to the highly porous structure. On the other hand, Fig. 6 (b) highlighted the remarkable performance of the FD-GO membranes. Among all the membranes prepared, the freeze-dried samples showed the lowest initial contact angles and the most significant decrease over time. This indicated superior hydrophilicity, making them the most water-affine membranes. One possible interpretation was that the freeze-drying process preserved most of the oxygen-containing functional groups in the GO, preventing the collapse or reduction of nanochannels within the membrane structure and thereby maintaining a highly hydrophilic surface (Ham et al., 2014; Wang et al., 2014). This preservation of functional groups can be crucial to interact readily with water molecules, leading to a more pronounced wettability compared to other drying methods. Another possible explanation is that the FD-GO was not strongly adhered to the MCE membrane, particularly at low GO content,

and thus remained readily dispersible in water. Accordingly, the FD-GO membrane detached from the support membrane over the time of the measurement and so that the final contact angles at longer durations reflected the hydrophilicity of the MCE substrate. In contrast, the VD-GO membranes, shown in Fig. 6 (c), exhibited slightly lower contact angles than the oven-dried samples. However, these membranes still maintained a relatively stable contact angle over time. The vacuum environment during oven drying may have preserved some of the oxygen-containing functional groups that would otherwise be reduced under conventional oven drying, resulting in a modest enhancement of hydrophilicity (Bayer et al., 2014). Despite this, the contact angles remained higher than those observed for pristine GO, indicating that the reduction in oxygen functionalities still played a significant role in providing more pathways within the membrane structure and hence determining the wettability of the membranes. In contrast, Fig. 6 (d) presented the dynamic contact angle measurements for GO membranes dried using normal oven drying (OD). The contact angles of these membranes remained relatively stable over time, suggesting a lower water affinity compared to pristine GO and FD-GO membranes. This reduced hydrophilicity was consistent with the partial loss of oxygen functional groups during the oven drying process (Huang et al., 2016). As the loss of these groups decreased the membrane's polar nature, its wettability decreased, leading to higher contact angles (Pei et al., 2016).

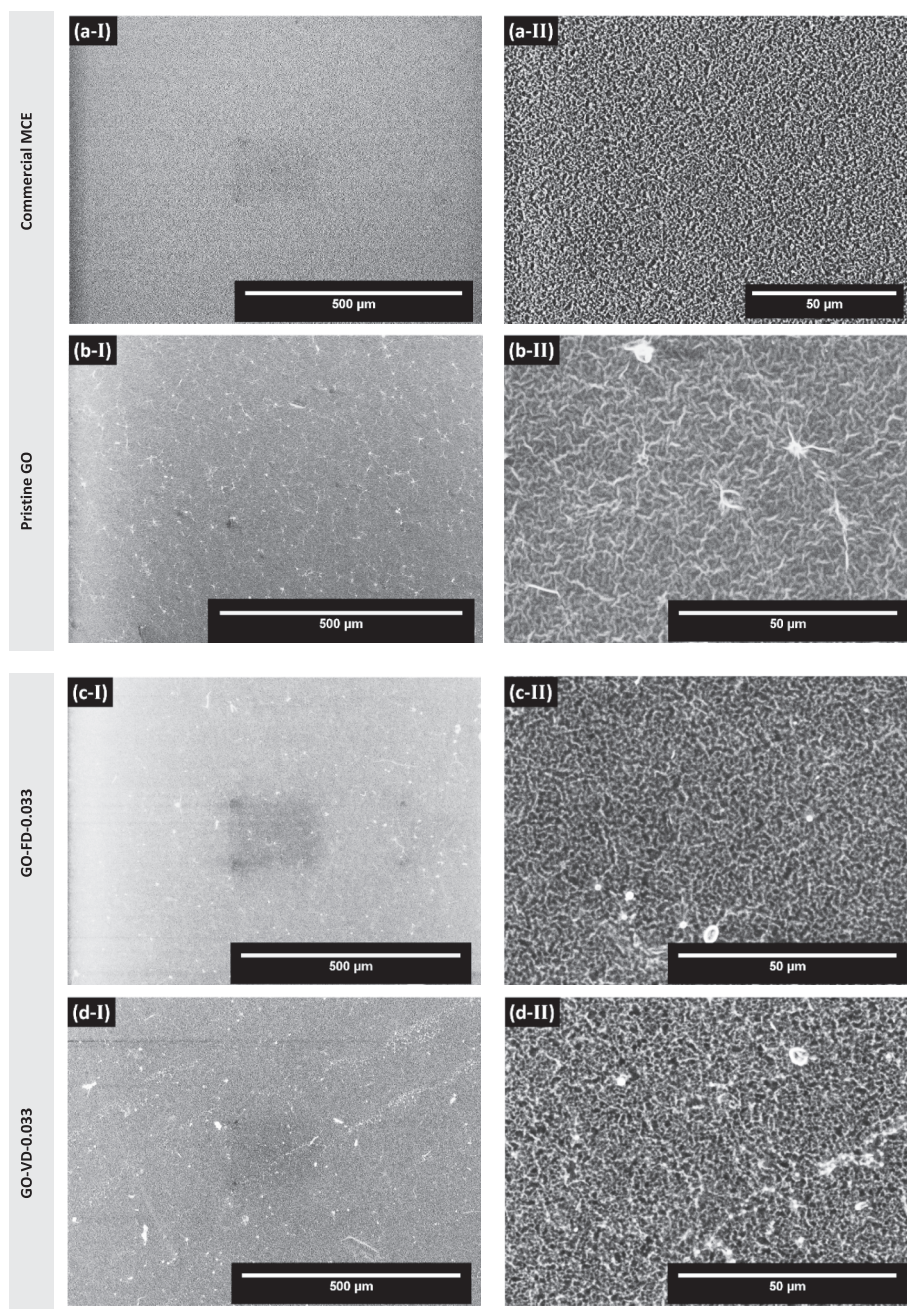


Fig. 5. SEM morphological characteristics for Pristine GO, Freeze-drying GO, Vacuum-drying GO, and Oven-drying GO.

Zeta potential (ZP) is a measure of the electrical surface charge of the membrane (Hurwitz et al., 2010). It is worth mentioning that the negative charge of all resultant GO-based membranes was due to the deprotonation of the carboxyl group of GO sheets in water (Fan et al., 2019). Across the ZP spectrum, as shown in Fig. 7 (a), all membranes exhibited negative zeta potentials, ranging from  $-22.1$  to  $-38.6$  mV, indicating negative surface charging, typical of GO materials. Notably, the more negative ZP values, particularly observed in FD and VD samples, might indicate surfaces with enhanced resistance to fouling due to stronger electrostatic repulsion of similarly charged foulants. However, the pressure drops measurements, reflecting the hydraulic resistance of the membranes, showed considerable variation from  $173.9$  to  $480.5$  mbar, as shown in Fig. 7 (b). These variations pointed to differences in membrane pore sizes and the degree of GO de-oxygenation, with higher pressure drops proposing either smaller pore sizes or reduction of d-

spacing and reduction of hydrophilicity. The results showed that OD-GO treatment typically resulted in higher pressure drops compared to FD-GO and VD-GO, possibly due to the denser packing, reduced pore sizes and wettability caused by this drying method. The comparative analysis of the different drying methods revealed that FD-GO tended to retain a more open pore structure and higher hydrophilicity, leading to lower pressure drops and slightly higher negative zeta potentials. In contrast, OD (and to some extent, VD) method could enhance the membrane's structural compactness leading to lower zeta potentials but higher pressure drops. These findings suggest that the choice of drying method can significantly influence the functional properties of GO membranes. These findings have important implications for tailoring membrane properties for specific applications, particularly in contexts where fouling resistance and hydraulic efficiency are critical, such as FO desalination (Wu et al., 2020).

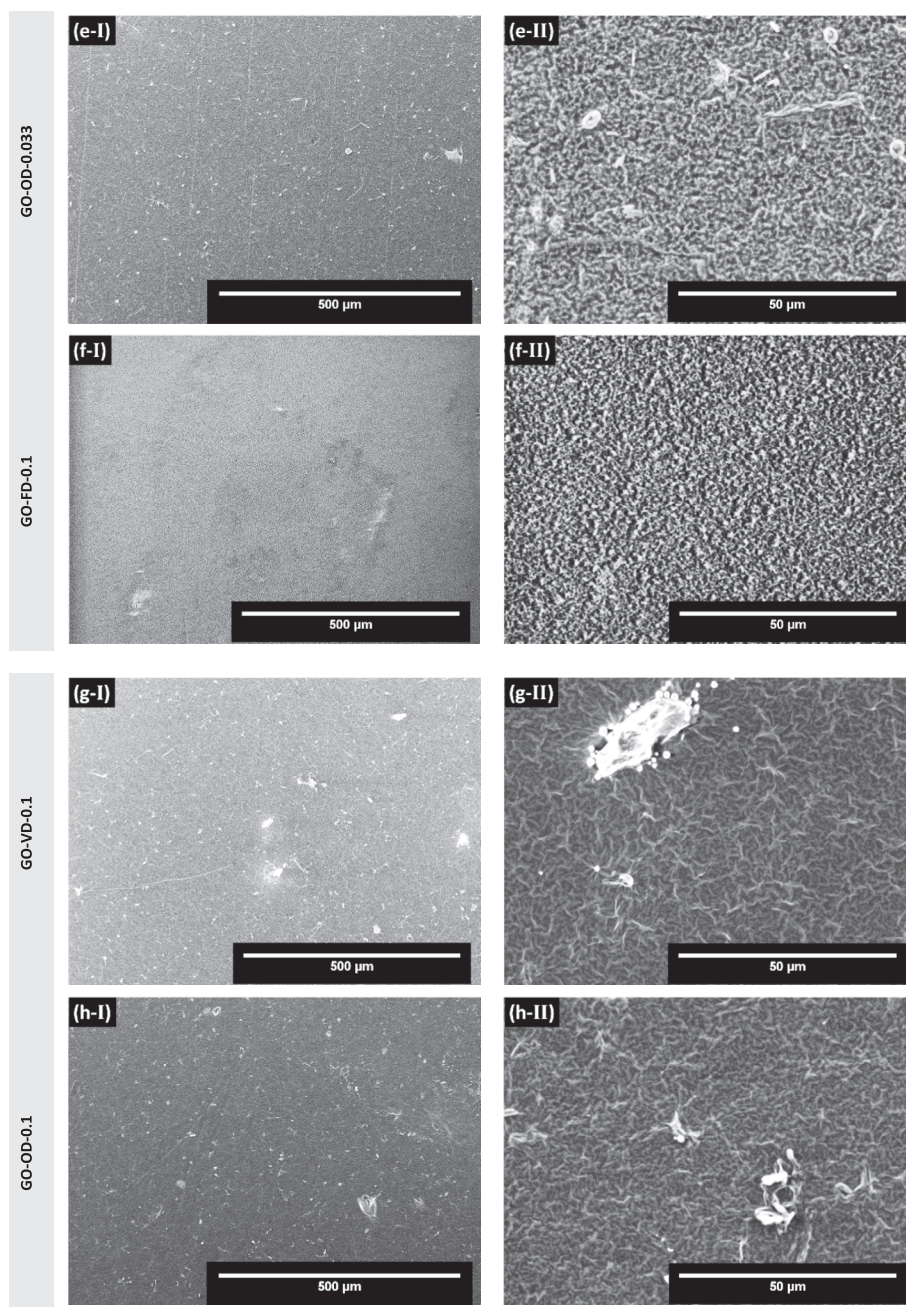


Fig. 5. (continued).

### 3.2. Desalination performance of membranes in an FO process

To evaluate the desalination performance of three differently-dried GO membranes in an FO system, 0.1 M NaCl and 0.5 M sucrose solutions were used as feed and draw solutions, respectively. Fig. 8 and Fig. 9 (supported by Table S3, SI) present a comprehensive analysis of water flux, salt rejection, and selectivity ratios for resultant GO membranes subjected to different drying methods; freeze-drying (FD), vacuum-oven drying (VD), and conventional oven-drying (OD) at varying concentrations of deposited GO films (0.033, 0.1, and 1 mg/mL) and volumes (2 mL and 4 mL). As observed, a general trend was evident across all drying methods with respect to GO concentration: increasing the membrane treatment volume from 2 to 4 mL resulted in a decrease in water flux. This effect can be attributed to increased membrane thickness and density, which may impede water flow as a result of higher volumes of deposited GO material. This observation is in good agreement with

findings reported in the literature (Edokali et al., 2023; Fan et al., 2019). Notably, results indicated that FD-GO membranes, characterised by their higher porosity and hydrophilicity due to rapid ice sublimation, exhibited the highest water flux, particularly at lower concentrations (e.g., GO-FD-0.033 at 2 mL:  $11.28 \pm 0.564$  LMH), with a decrease as concentration and volume increased (e.g., rGO-FD-1 at 4 mL:  $4.54 \pm 0.227$  LMH), resulting in reducing pressure drops across the FD-GO membranes. These findings agreed with the obtained results of XRD, SEM, ZP, and WCA. In comparison, VD-GO membranes showed moderate rates of water flux and salt rejection, indicating partial structural densification due to moisture removal under reduced pressure (e.g., GO-VD-1 at 4 mL:  $3.75 \pm 0.187$  LMH with  $99.53 \pm 0.239$  % salt rejection). Contrastingly, The OD-GO membranes, which exhibited the lowest water flux (e.g., GO-OD-1 at 4 mL:  $2.83 \pm 0.141$  LMH), achieved the highest salt rejection (up to  $99.67 \pm 0.249$  %) and selectivity ( $R/J_w$  peaking at 35.2). This performance was attributed to their compact

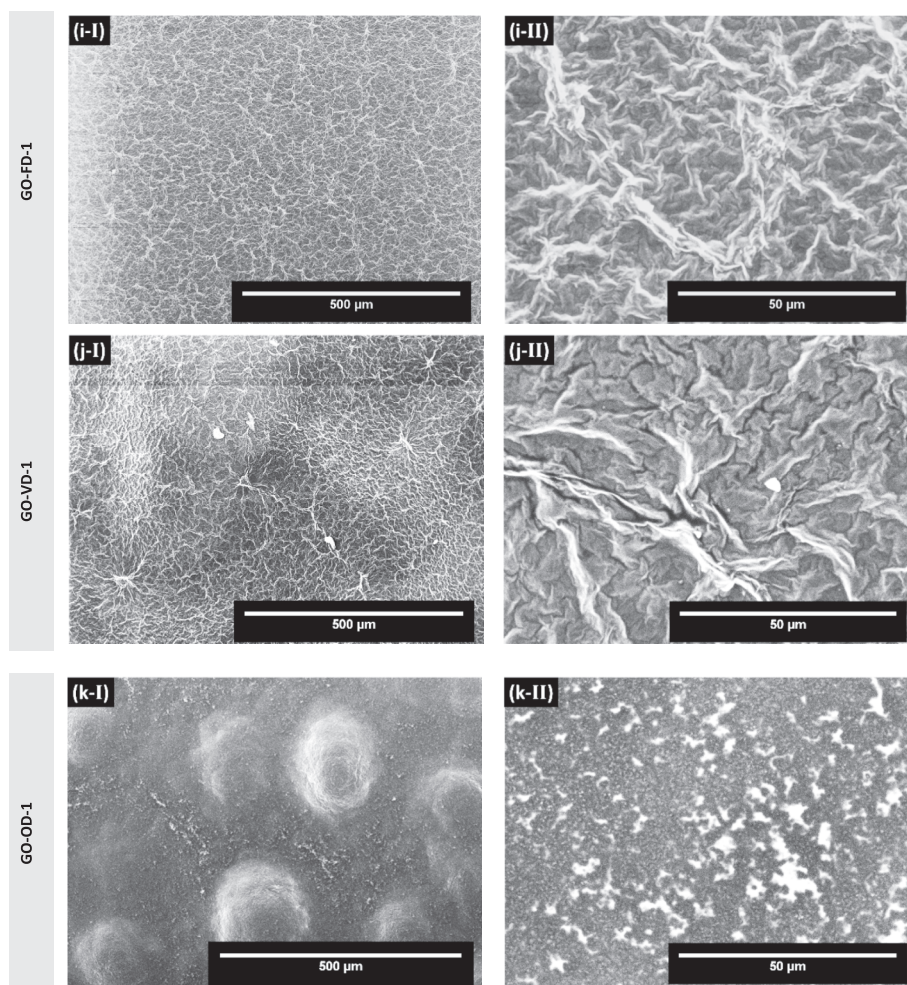


Fig. 5. (continued).

structure formed through gradual moisture loss and enhanced compaction, which was consistent with the FTIR, XRD, SEM, and WCA results. The data implied that freeze-drying promoted a porous structure conducive to water transport, while vacuum drying balanced performance, and oven drying enhanced salt rejection due to the significant reduction of interlayer spacing. These trends were consistent with the characterization results, which indicate that FD-GO membranes offered higher flux due to their looser morphology and preservable wet structure, whereas oven drying promoted tighter packing, thereby enhancing ion exclusion. The performance of GO membranes in the FO process is also significantly influenced by the negative charges inherent to their surface. The negatively charged functional groups present on the GO membranes enhanced their hydrophilicity, facilitating increased water transport and effective ion rejection through electrostatic repulsion (Parsamehr et al., 2019; Yang et al., 2017; Yu et al., 2010). This characteristic was particularly impactful in FO desalination, where the electrostatic repulsion between the negatively charged GO surface and chloride ions contributed to enhanced salt rejection. Variations in drying methods influenced the extent of negative charge retention, thereby affecting overall membrane performance. These trends are consistent with the reported literature, which highlighted that the interplay between membrane porosity and surface charge governed the balance between water permeability and salt rejection (Edokali et al., 2024). Consequently, the drying method plays a critical role in tailoring membrane performance by influencing the structural attributes and permeability of GO membranes.

Despite the growing interest in GO-based membranes for water

desalination, limited attention has been paid to the performance of additive-free, non-chemically modified GO membranes, particularly in the context of FO applications. Much of the existing literature has focused on chemically enhanced membranes or hybrid systems with polymeric or nanoparticle modifications to achieve desirable performance. However, our study advances from these approaches by investigating pristine GO membranes, fabricated without additives or chemical crosslinking, and places strong emphasis on the influence of drying time and temperature as critical yet often overlooked parameters affecting membrane performance and structure.

The comparative data provided in Table 1 clearly illustrates this distinction. For instance, membranes reported in Yang et al. (Yang et al., 2018) and Padmavathy et al. (Padmavathy et al., 2019) employed vacuum-dried GO active layers supported on chemically treated substrates, operating at long drying durations (24–8 hrs.), and delivered moderate to high water flux rates (17.2 LMH and 95 LMH, respectively) with salt rejection ranging from 35 % to 85 %. Edokali et al. (Edokali et al., 2023) used a polydopamine-modified nylon substrate with GO and vacuum-dried at 2.5 hrs., yielding improved salt rejection (88.2 %) but moderate flux (33 LMH). In contrast, the FD GO membranes in this work (FD, 4 hrs.) fabricated with a significantly lower concentration (0.033 mg/mL) not only achieved a comparable water flux of 11.2 LMH but also demonstrated high salt rejection (97.2 %), without any chemical modification. Notably, in the current study freeze-drying (FD) was systematically investigated as a drying strategy for GO membranes in FO desalination. The FD approach demonstrated promise by preserving GO's interlayer spacing (0.78 nm), maintaining structural integrity, and

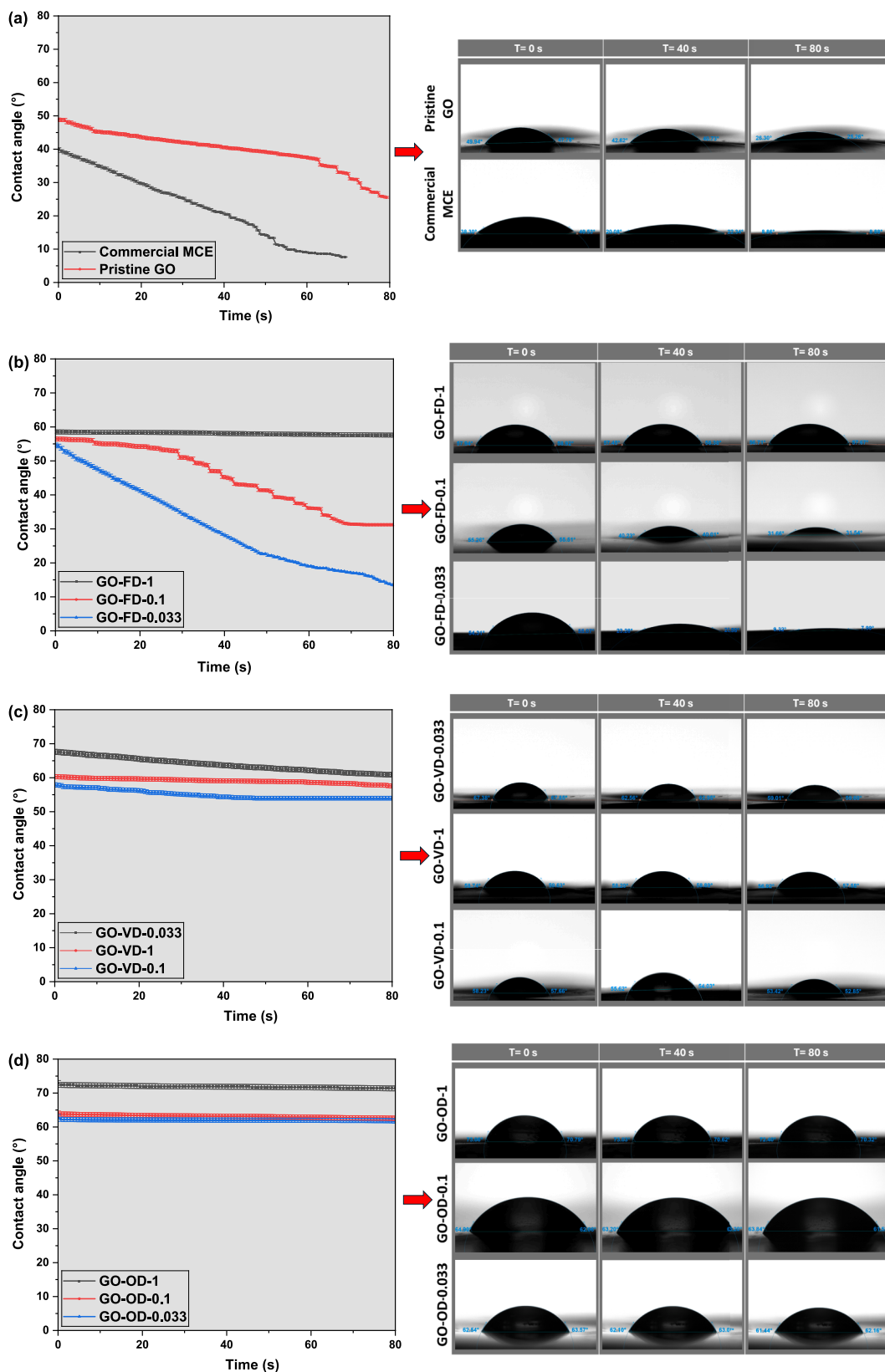


Fig. 6. Dynamic contact angle measurements of water droplets on the (a) pristine GO and Commercial MCE membranes, (b) freeze-dried, (c) vacuum-dried, and (d) oven-dried GO membranes.

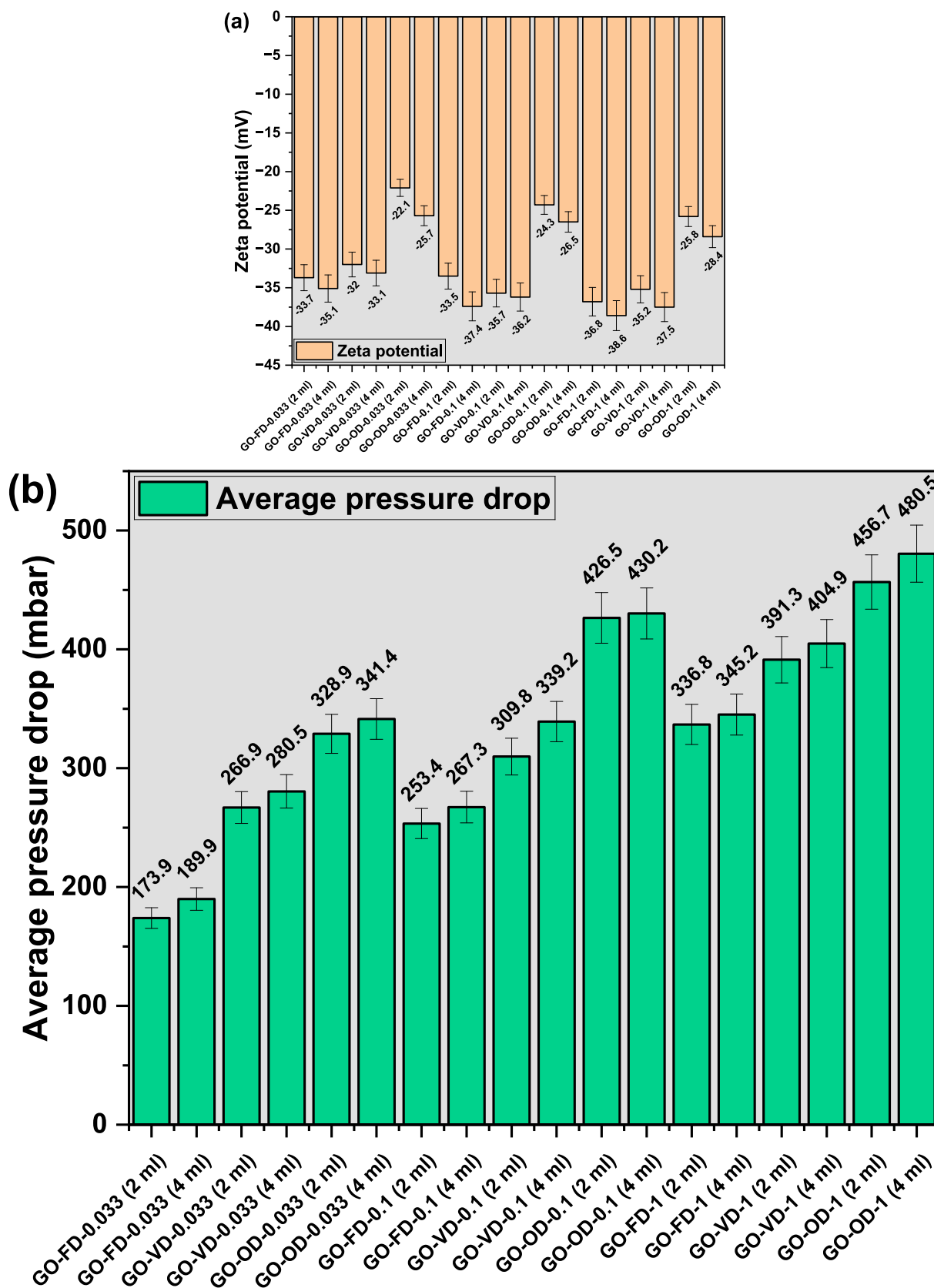


Fig. 7. (a) Surface charge-(ZP) and (b) average pressure drop of GO-based membranes for all drying methods.

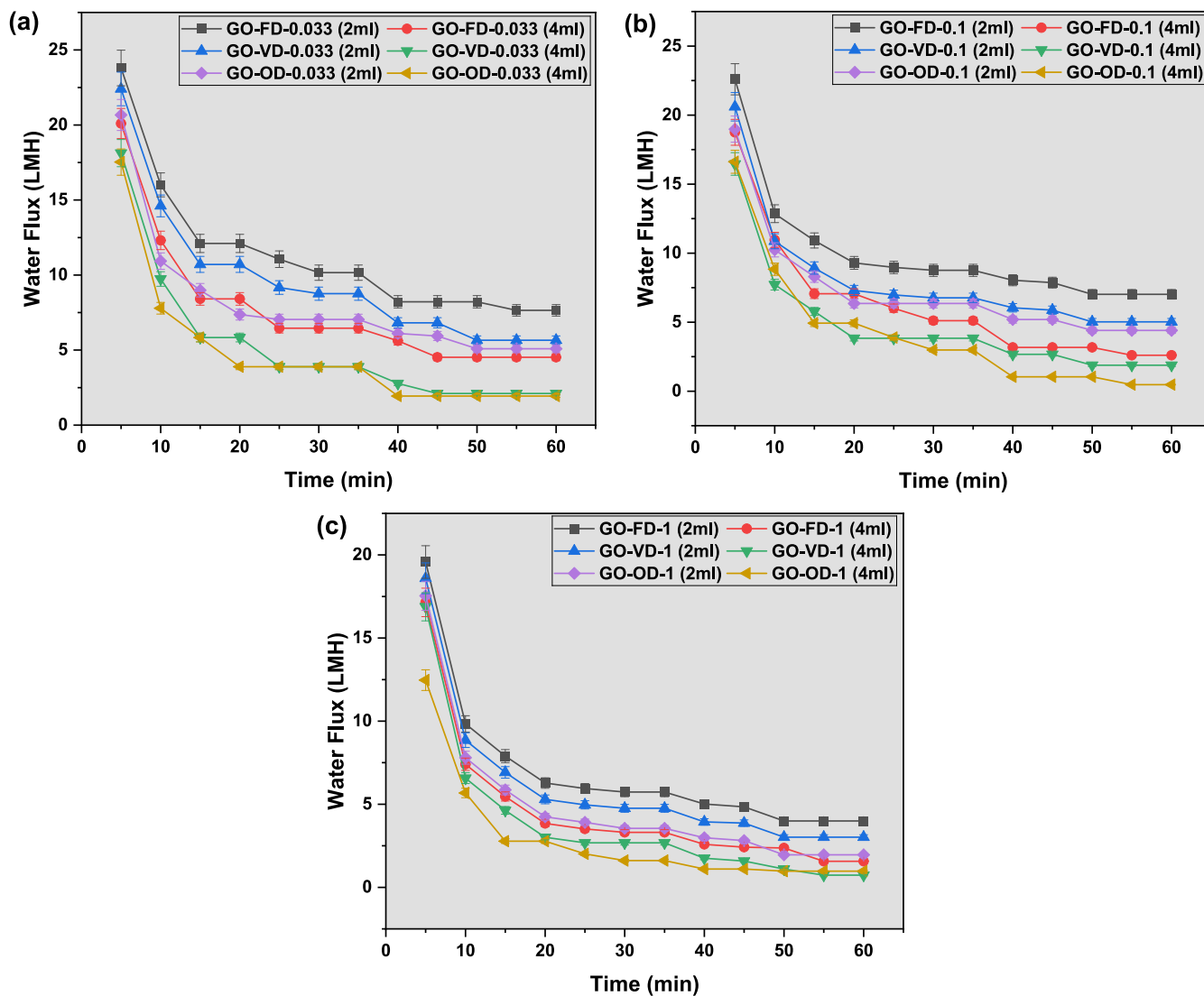


Fig. 8. Dynamic water flux performance across dried GO membranes: comparing the impact of freeze-drying, vacuum-drying, and oven-drying methods at concentrations of (a) 0.033, (b) 0.1, and (c) 1 mg/ml.

enhancing water transport pathways.

Furthermore, while this work systematically optimised the drying parameters and operating conditions, it is important to note that the effect of GO active layer thickness, though known to significantly influence membrane transport properties, was not fully explored at this stage. Thickness is intrinsically linked to deposition volume and concentration, and its precise quantification will be a focus of future research. Our results establish that the drying method, time, and temperature, rather than chemical functionalisation, can be indicated as effective tools to tailor membrane performance, paving the way for more sustainable, scalable, and high-performance GO-based membranes for water desalination.

#### 4. Conclusion

In this study, three drying methods were employed to fabricate additive-free GO membranes, and their characteristics and performance in FO were comprehensively compared. The drying method had a significant influence on the membrane properties: freeze-drying preserved the structural integrity and hydrophilicity; vacuum-drying led to moderate deoxygenation and retained a reasonable level of hydrophilicity, while oven-drying resulted in the highest degree of compaction and

markedly reduced wettability. In addition, the effect of the drying methods was noticed through the outcomes achieved, where the FD-GO membranes, whose preservation of nano-porous structure was noticeably seen through its scanned surface morphology, performed the best among the other drying methods (i.e., OD and VD), accomplishing the highest water flux of nearly  $11.28 \text{ L/m}^2\text{h}$  at a lower concentration of  $0.033 \text{ mg/ml}$ , which promoted an efficient water movement mechanism. On the other hand, OD-GO membranes attained the highest salt rejection percentage, achieving a salt rejection percentage of up to 99.67% at a higher concentration of  $1 \text{ mg/mL}$ , emphasising their super efficiency in yielding a high percentage of water purification. These findings underscore the critical role of carefully selected drying methods, which can significantly influence the optimisation of GO membranes for forward osmosis applications, either positively or negatively. More importantly, utilising the optimal drying process can greatly affect the structural integrity of the membrane materials, and could also contribute to improve the qualitative and quantitative efficiency in the field of FO water desalination through the preservation of eco-environmental sustainability to achieve high filtration standards without using further chemical modification approaches. Although the operational time in this study was limited to 60 mins, it provided critical insights into how drying methods influence the short-term performance

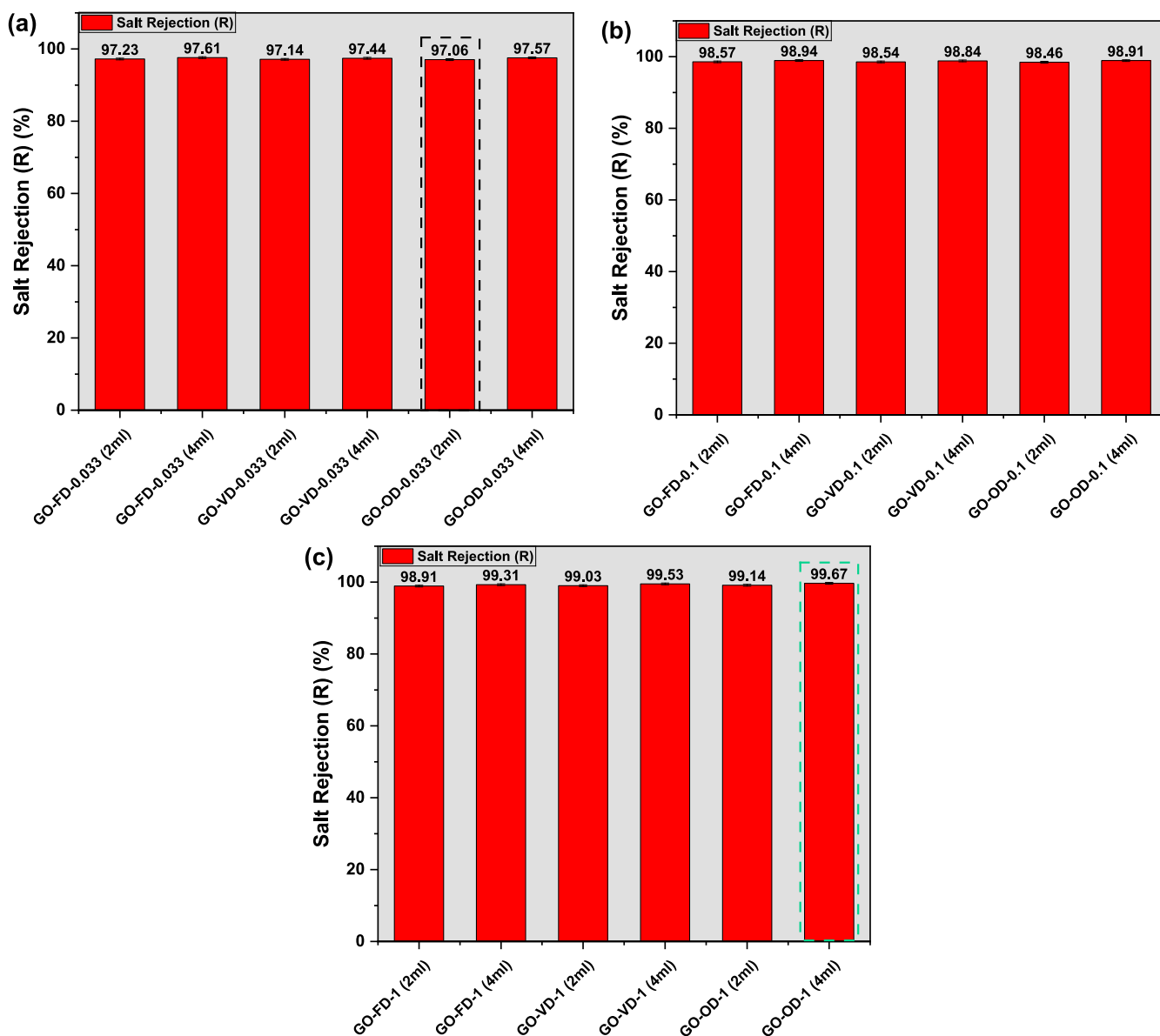


Fig. 9. Salt rejection across dried GO membranes: comparative analysis of freeze-drying, vacuum-drying, and oven-drying methods at concentrations of 0.033, 0.1, and 1 mg/ml. [Inset dashed **black** line shows the lowest value while the inset dashed **green** line indicates the highest value].

Table 1

Comparative performance of additive-free GO membranes fabricated via different drying methods for FO desalination.

Membrane (Active(Con.)/Support)	Fabrication Technique	Drying method/Time	d-spacing (nm)	FO desalination performance			Ref.
				Filtration time (hr.)	Water flux (LMH)	NaCl Salt rejection (%)	
GO-1 mg/ml/MCE	Vacuum-filtration	RT (24 hrs.)	0.76	1	17.2	35	(Yang et al., 2018)
GO-0.5 mg/ml/PVDF	Vacuum-filtration	VD (8 hrs.)	0.8	24	95	85	(Padmavathy et al., 2019)
GO-0.5 mg/ml/pDA-Nylon	Vacuum-filtration	VD (2.5 hrs.)	0.76	3	33	88.2	(Edokali et al., 2023)
GO-0.033 mg/ml/MCE	Vacuum-filtration	VD (4 hrs.)	0.74	1	9.6	97.1	This work
GO-0.1 mg/ml/MCE	Vacuum-filtration	OD (2 hrs.)	0.7	1	7.2	98.4	This work
GO-0.033 mg/ml/MCE	Vacuum-filtration	FD (4 hrs.)	0.78	1	11.2	97.2	This work

and structural stability of unmodified GO membranes. Our future investigations will extend these findings by:

- Evaluating the long-term operational stability and antifouling performance of GO membranes using model foulants under realistic FO desalination conditions.

- Further refining the freeze-drying technique for scalability, with the goal of enhancing the performance and industrial applicability of GO-based membranes.
- Investigating the underlying mechanisms governing the improved properties of FD GO membranes, particularly those treated with plasma, to establish them as a robust and sustainable solution for FO water purification.
- Exploring a fully chemical-free surface modification approach using plasma treatment, aimed at improving hydrophilicity, interlayer spacing, and mechanical integrity of GO membranes.
- Translating the promising results of this study into the development of next-generation FO membranes, with potential impact in water-stressed regions affected by scarcity and contamination.

### CRedit authorship contribution statement

**Abdulhakim Alhinai:** Writing – original draft, Methodology, Investigation, Formal analysis. **Mohamed Edokali:** Writing – review & editing, Methodology, Investigation, Formal analysis, Data curation, Conceptualization. **Louey Tliba:** Writing – review & editing, Methodology, Investigation, Formal analysis, Data curation. **Robert Menzel:** Writing – review & editing, Supervision, Investigation. **Ali Hassanpour:** Writing – review & editing, Supervision, Investigation, Formal analysis.

### Declaration of competing interest

The authors declare that they have no known competing financial interests or personal relationships that could have appeared to influence the work reported in this paper.

### Acknowledgment

The authors would like to acknowledge the financial support from Ministry of Higher Education and Scientific Research – Oman for the Masar Watan scholarship program. We also thank the Ministry of Higher Education and Scientific Research – State of Libya for the funding support. Besides, we acknowledge the technical support provided by Dr Ben Douglas from the school of chemical and process engineering (University of Leeds), and Dr Christopher Pask from school of chemistry (University of Leeds).

### Appendix A. Supplementary data

Supplementary data to this article can be found online at <https://doi.org/10.1016/j.ces.2025.121998>.

### Data availability

Data will be made available on request.

### References

- Abraham, J., Vasu, K.S., Williams, C.D., Gopinadhan, K., Su, Y., Cherian, C.T., Dix, J., Prestat, E., Haigh, S.J., Grigorieva, I.V., 2017. Tunable sieving of ions using graphene oxide membranes. *Nat. Nanotechnol.* 12 (6), 546.
- Allahbakhsh, A., Arjmand, M., 2019. Graphene-based phase change composites for energy harvesting and storage: state of the art and future prospects. *Carbon* 148, 441–480.
- Balapanuru, J., Manga, K.K., Fu, W., Abdelwahab, I., Zhou, G., Li, M., Lu, H., Loh, K.P., 2019. Desalination properties of a free-standing, partially oxidized few-layer graphene membrane. *Desalination* 451, 72–80.
- Bayer, T., Bishop, S., Nishihara, M., Sasaki, K., Lyth, S., 2014. Characterization of a graphene oxide membrane fuel cell. *J. Power Sources* 272, 239–247.
- Castelletto, S., Boretti, A., 2021. Advantages, limitations, and future suggestions in studying graphene-based desalination membranes. *RSC Adv.* 11 (14), 7981–8002.
- Chen, L., Shi, G., Shen, J., Peng, B., Zhang, B., Wang, Y., Bian, F., Wang, J., Li, D., Qian, Z., 2017. Ion sieving in graphene oxide membranes via cationic control of interlayer spacing. *Nature* 550 (7676), 380–383.
- Chong, J., Wang, B., Li, K., 2016. Graphene oxide membranes in fluid separations. *Curr. Opin. Chem. Eng.* 12, 98–105.
- Deka, P., Verma, V.K., Yurembam, B., Neog, A.B., Raidongia, K., Subbiah, S., 2021. Performance evaluation of reduced graphene oxide membrane doped with polystyrene sulfonic acid for forward osmosis process. *Sustainable Energy Technol. Assess.* 44, 101093.
- Dreyer, D.R., Park, S., Bielawski, C.W., Ruoff, R.S., 2010. The chemistry of graphene oxide. *Chem. Soc. Rev.* 39 (1), 228–240.
- Edokali, M., Bocking, R., Mehrabi, M., Massey, A., Harbottle, D., Menzel, R., Hassanpour, A., 2023. Chemical modification of reduced graphene oxide membranes: enhanced desalination performance and structural properties for forward osmosis. *Chem. Eng. Res. Des.*
- Edokali, M., Mehrabi, M., Cespedes, O., Sun, C., Collins, S.M., Harbottle, D., Menzel, R., Hassanpour, A., 2024. Antifouling and stability enhancement of electrochemically modified reduced graphene oxide membranes for water desalination by forward osmosis. *J. Water Process Eng.* 59, 104809.
- Edokali, M., Bocking, R., Massey, A., Al Hinai, A., Harbottle, D., Menzel, R., Hassanpour, A., 2024. Effect of polymer-entwined reduced graphene oxide laminates on the performance and stability of forward osmosis membranes for water desalination. *Polymer* 312, 127644.
- Fan, X., Liu, Y., Quan, X., 2019. A novel reduced graphene oxide/carbon nanotube hollow fiber membrane with high forward osmosis performance. *Desalination* 451, 117–124.
- Gao, W., Alemany, L.B., Ci, L., Ajayan, P.M., 2009. New insights into the structure and reduction of graphite oxide. *Nat. Chem.* 1 (5), 403–408.
- Ghahari, N., Ramezan, Y., Mirsaedghazi, H., Faraji, A., 2024. Clarification of apple juice using cold plasma treated mixed cellulose esters membrane: flux modeling, membrane fouling, and juice physicochemical properties evaluation. *LWT*, 116951.
- Goh, P., Matsuura, T., Ismail, A., Hilal, N., 2016. Recent trends in membranes and membrane processes for desalination. *Desalination* 391, 43–60.
- Ham, H., Van Khai, T., Park, N.-H., So, D.S., Lee, J.-W., Na, H.G., Kwon, Y.J., Cho, H.Y., Kim, H.W., 2014. Freeze-drying-induced changes in the properties of graphene oxides. *Nanotechnology* 25 (23), 235601.
- Huang, L., Chen, J., Gao, T., Zhang, M., Li, Y., Dai, L., Qu, L., Shi, G., 2016. Reduced graphene oxide membranes for ultrafast organic solvent nanofiltration. *Adv. Mater.* 28 (39), 8669–8674.
- Huang, G., Ghalei, B., Pournaghshband Isfahani, A., Karahan, H.E., Terada, D., Qin, D., Li, C., Tsujimoto, M., Yamaguchi, D., Sugimoto, K., 2021. Overcoming humidity-induced swelling of graphene oxide-based hydrogen membranes using charge-compensating nanodiamonds. *Nat. Energy* 6 (12), 1176–1187.
- Hurwitz, G., Guillen, G.R., Hoek, E.M., 2010. Probing polyamide membrane surface charge, zeta potential, wettability, and hydrophilicity with contact angle measurements. *J. Membr. Sci.* 349 (1–2), 349–357.
- Ibraheem, B.M., Aani, S.A., Alsarayreh, A.A., Alsalhy, Q.F., Salih, I.K., 2023. Forward osmosis membrane: review of fabrication, modification, challenges and potential. *Membranes* 13 (4), 379.
- Jabbari, A., Ghanbari, H., Naghizadeh, R., 2023. Partial reduction of graphene oxide toward the facile fabrication of desalination membrane. *Int. J. Environ. Sci. Technol.* 20 (1), 831–842.
- Jang, J., Park, I., Chee, S.-S., Song, J.-H., Kang, Y., Lee, C., Lee, W., Ham, M.-H., Kim, I.S., 2020. Graphene oxide nanocomposite membrane cooperatively cross-linked by monomer and polymer overcoming the trade-off between flux and rejection in forward osmosis. *J. Membr. Sci.* 598, 117684.
- Joshi, R., Carbone, P., Wang, F.-C., Kravets, V.G., Su, Y., Grigorieva, I.V., Wu, H., Geim, A.K., Nair, R.R., 2014. Precise and ultrafast molecular sieving through graphene oxide membranes. *Science* 343 (6172), 752–754.
- Kamal, M., Abdelrazek, E., Sellow, N., Abdelghany, A., 2018. Synthesis and optimization of novel chitosan/cellulose acetate natural polymer membrane for water treatment. *J. Adv. Phys* 14 (1), 5303–5311.
- Kim, S., Lin, X., Ou, R., Liu, H., Zhang, X., Simon, G.P., Easton, C.D., Wang, H., 2017. Highly crosslinked, chlorine tolerant polymer network entwined graphene oxide membrane for water desalination. *J. Mater. Chem. A* 5 (4), 1533–1540.
- Li, M.-L., Hou, D.-F., Li, P.-Y., Feng, Z.-W., Huang, Y.-H., Wang, F., Zhai, Y.-M., Sun, X.-R., Zhang, K., Yin, B., 2024. One-Step Solvent-Free Strategy to Efficiently Synthesize High-Substitution Cellulose Esters. *ACS Sustain. Chem. Eng.*
- Li, W., Wu, W., Li, Z., 2018. Controlling interlayer spacing of graphene oxide membranes by external pressure regulation. *ACS Nano* 12 (9), 9309–9317.
- Liu, H., Wang, H., Zhang, X., 2015. Facile fabrication of freestanding ultrathin reduced graphene oxide membranes for water purification. *Adv. Mater.* 27 (2), 249–254.
- Marchetti, P., Jimenez Solomon, M.F., Szekely, G., Livingston, A.G., 2014. Molecular separation with organic solvent nanofiltration: a critical review. *Chem. Rev.* 114 (21), 10735–10806.
- Meng, Z., Casanova, S., Mohamed, H., Kapil, N., Xiao, X., Zhang, Y., Coppens, M.-O., Mattia, D., 2020. Polymer nanotube membranes synthesized via liquid deposition in anodic alumina. *Colloid Interface Sci. Commun.* 39, 100334.
- Mohiuddin, M., Sadasivuni, K.K., Mun, S., Kim, J., 2015. Flexible cellulose acetate/graphene blueprints for vibrotactile actuator. *RSC Adv.* 5 (43), 34432–34438.
- Nde, D., Appiah-Kubi, M., Watt, J., Watanabe, F., Zhao, W., 2023. Tuning Fabrication Factors for Reduced Graphene Oxide Forward Osmosis Membranes. *J. Phys. Chem. C*.
- Ndiaye, I., S. Vaudreuil, and T. Bounahmidi, *Forward Osmosis Process: State-Of-The-Art of Membranes. Separation & Purification Reviews*, 2019: p. 1-21.
- Padmavathy, N., Behera, S.S., Pathan, S., Das Ghosh, L., Bose, S., 2019. Interlocked graphene oxide provides narrow channels for effective water desalination through forward osmosis. *ACS Appl. Mater. Interfaces* 11 (7), 7566–7575.
- Parsamehr, P.S., Zahed, M., Tofighy, M.A., Mohammadi, T., Rezakazemi, M., 2019. Preparation of novel cross-linked graphene oxide membrane for desalination

- applications using (EDC and NHS)-activated graphene oxide and PEI. *Desalination* 468, 114079.
- Pei, J., Zhang, X., Huang, L., Jiang, H., Hu, X., 2016. Fabrication of reduced graphene oxide membranes for highly efficient water desalination. *RSC Adv.* 6 (104), 101948–101952.
- Salehi, H., Rastgar, M., Shakeri, A., 2017. Anti-fouling and high water permeable forward osmosis membrane fabricated via layer by layer assembly of chitosan/graphene oxide. *Appl. Surf. Sci.* 413, 99–108.
- Song, J.-H., Shon, H.K., Wang, P., Jang, A., Kim, I.S., 2019. Tuning the nanostructure of nitrogen-doped graphene laminates for forward osmosis desalination. *Nanoscale* 11 (45), 22025–22032.
- Su, P., Wang, F., Li, Z., Tang, C.Y., Li, W., 2020. Graphene oxide membranes: controlling their transport pathways. *J. Mater. Chem. A* 8 (31), 15319–15340.
- Surwade, S.P., Smirnov, S.N., Vlasiouk, I.V., Unocic, R.R., Veith, G.M., Dai, S., Mahurin, S.M., 2015. Water desalination using nanoporous single-layer graphene. *Nat. Nanotechnol.* 10 (5), 459–464.
- Talar, A.J., Ebadi, T., Maknoon, R., Rashidi, A., 2019. Investigation on effect of KCl addition on desalination performance of co-polymerized GO/Nylon nanocomposite membrane. *Process Saf. Environ. Prot.* 125, 31–38.
- Tian, L., Jiang, Y., Li, S., Han, L., Su, B., 2020. Graphene oxide interlayered thin-film nanocomposite hollow fiber nanofiltration membranes with enhanced aqueous electrolyte separation performance. *Sep. Purif. Technol.* 248, 117153.
- Wang, J., Gao, X., Wang, Y., Gao, C., 2014. Novel graphene oxide sponge synthesized by freeze-drying process for the removal of 2, 4, 6-trichlorophenol. *RSC Adv.* 4 (101), 57476–57482.
- Wang, X., Mao, Y.-F., Shen, X., Zhao, J., Zhou, J., Liu, Z., 2023. Advances and prospects in graphene oxide membranes for seawater salt ion sieving and rejection. *Sep. Purif. Technol.*, 125216.
- Warsinger, D.M., Chakraborty, S., Tow, E.W., Plumlee, M.H., Bellona, C., Loutatidou, S., Karimi, L., Mikelonis, A.M., Achilli, A., Ghassemi, A., 2018. A review of polymeric membranes and processes for potable water reuse. *Prog. Polym. Sci.* 81, 209–237.
- Wu, W., Shi, Y., Liu, G., Fan, X., Yu, Y., 2020. Recent development of graphene oxide based forward osmosis membrane for water treatment: A critical review. *Desalination* 491, 114452.
- Xiao, X., Li, S., Zhu, X., Xiao, X., Zhang, C., Jiang, F., Yu, C., Jiang, L., 2021. Bioinspired two-dimensional structure with asymmetric wettability barriers for unidirectional and long-distance gas bubble delivery underwater. *Nano Lett.* 21 (5), 2117–2123.
- Yang, E., Kim, C.-M., Song, J.-H., Ki, H., Ham, M.-H., Kim, I.S., 2017. Enhanced desalination performance of forward osmosis membranes based on reduced graphene oxide laminates coated with hydrophilic polydopamine. *Carbon* 117, 293–300.
- Yang, E., Alayande, A.B., Kim, C.-M., Song, J.-H., Kim, I.S., 2018. Laminar reduced graphene oxide membrane modified with silver nanoparticle-polydopamine for water/ion separation and biofouling resistance enhancement. *Desalination* 426, 21–31.
- Yang, L., Xiao, X., Shen, S., Lama, J., Hu, M., Jia, F., Han, Z., Qu, H., Huang, L., Wang, Y., 2022. Recent advances in graphene oxide membranes for nanofiltration. *ACS Appl. Nano Mater.* 5 (3), 3121–3145.
- Yu, B., Liu, J., Liu, S., Zhou, F., 2010. Pdp layer exhibiting zwitterionicity: a simple electrochemical interface for governing ion permeability. *Chem. Commun.* 46 (32), 5900–5902.
- Yuan, Y., Gao, X., Wei, Y., Wang, X., Wang, J., Zhang, Y., Gao, C., 2017. Enhanced desalination performance of carboxyl functionalized graphene oxide nanofiltration membranes. *Desalination* 405, 29–39.
- Zhang, Z., Xiao, X., Zhou, Y., Huang, L., Wang, Y., Rong, Q., Han, Z., Qu, H., Zhu, Z., Xu, S., 2021. Bioinspired graphene oxide membranes with pH-responsive nanochannels for high-performance nanofiltration. *ACS Nano* 15 (8), 13178–13187.
- Zhao, S., Zou, L., Tang, C.Y., Mulcahy, D., 2012. Recent developments in forward osmosis: opportunities and challenges. *J. Membr. Sci.* 396, 1–21.
- Zhu, L., Guo, X., Chen, Y., Chen, Z., Lan, Y., Hong, Y., Lan, W., 2022. Graphene oxide composite membranes for water purification. *ACS Appl. Nano Mater.* 5 (3), 3643–3653.
- Zhu, X., Yu, Z., Zeng, H., Feng, X., Liu, Y., Cao, K., Li, X., Long, R., 2021. Using a simple method to prepare UiO-66-NH<sub>2</sub>/chitosan composite membranes for oil–water separation. *J. Appl. Polym. Sci.* 138 (31), 50765.